Physical-Ecological Response of the California Current System to ENSO events in ROMS-NEMURO

Nathalí Cordero-Quirós[1] · Arthur J. Miller[2] · Yunchun Pan[3] · Lawrence Balitaan[3] · Enrique Curchitser[4] · Raphael Dussin[5]

Abstract

We analyze the bottom-up El Niño/Southern Oscillation (ENSO) driven physical-biological response of the California Current System (CCS) in a high-resolution, "eddy-scale" ocean model with multiple classes of phytoplankton and zooplankton forced with observed winds over the time period 1959–2007. The response of the sea surface temperature anomalies over the CCS is asymmetrical, with La Niña events being more consistently cold than El Niño events are consistently warm, which is in agreement with previous studies. The biogeochemical and ecological response is represented by ENSO composite anomalies, lag correlations with an ENSO index, and histograms for ENSO years. The results show trophic level interactions during El Niño and La Niña events in which the larger components (diatoms, euphausiids, and copepods) are suppressed in the coastal upwelling zones during El Niño, while the smaller components (flagellates and ciliates) are enhanced. In addition, standing eddies of the CCS modulate the latitudinal structure of the ecological response to ENSO. The results point towards future research to understand how bottom-up changes may lead to variability of patterns in ecological response, including fish populations and top predators.

Keywords ENSO composite · CCS · Mesoscale · Upwelling · Bottom-up biophysical interactions

1 Introduction

The California Current System (CCS) is one of the major Eastern Boundary Upwelling Systems (EBUS) in the world (e.g., Hickey 1998; Checkley and Barth 2009; Miller et al. 2015). The seasonal longshore winds drive strong upwelling that ranges from northern Baja California, Mexico, up to Washington state along the North American West Coast (e.g., Bakun et al. 2015). This basic state renders a highly

✉ Nathalí Cordero-Quirós
ncorder1@ucsc.edu

[1] Institute of Marine Sciences, University of California, Santa Cruz, CA, USA

[2] Scripps Institution of Oceanography, University of California, San Diego, CA, USA

[3] University of California, San Diego, CA, USA

[4] Department of Environmental Sciences, Rutgers University, New Brunswick, NJ, USA

[5] Geophysical Fluid Dynamics Laboratory, Princeton, NJ, USA

productive regional ecosystem that is sensitive to both locally forced and remotely driven changes in atmospheric and oceanic flows. Part of that variability is due to atmospheric and oceanic teleconnections from the equatorial Pacific due to the major climate events of the El Niño/Southern Oscillation (ENSO), which imprints its signature in coastal upwelling, sea surface temperature (SST), horizontal advection, pycnocline depth, surface-heat and freshwater fluxes, and oceanic eddy statistics, among other fields (e.g., Jacox et al. 2015). Each of these physical processes can serve as a driver for changes in ecological conditions and biogeochemical properties that affect the overall state of the ecosystem on ENSO timescales (e.g., Schwing et al. 2005; Jacox et al. 2020).

Two distinct large-scale mechanisms are associated with ENSO affecting the CCS. One is the local effect of atmospheric forcing that is influenced by changes in the Aleutian Low during fall and winter and the North Pacific High in spring and summer during ENSO events (e.g., Alexander et al. 2002; Jacox et al. 2015), which alters upwelling favorable winds along the California coast. The other is the remote effect due to oceanic baroclinic Kelvin-wave-like

propagation along the coast into the CCS from southern latitudes where they are generated during ENSO events (e.g., McPhaden et al. 1998; Frischknecht et al. 2015). The mixture of these locally forced atmospheric changes and remotely forced ocean wave arrivals results in the key oceanic adjustment processes on interannual timescales that must be understood to characterize the imprint of ENSO on the CCS.

Since some aspects of ENSO are predictable over (at least) seasonal timescales, it is interesting to consider whether such predictive skill can be exploited in practical situations for such things as CCS oceanic fisheries (e.g., Jacox et al. 2020). In particular, there are many observational studies that link changes in the physical oceanographic environment to ecological response associated with ENSO events in the CCS (e.g., Bograd and Lynn 2001; Chávez et al. 2002; Jacox et al. 2016). Many of these efforts relied on datasets that were acquired over many decades by the California Cooperative Oceanic Fisheries Investigations (CalCOFI) program in the southern CCS (e.g., Gallo et al. 2019) and during the GLOBEC years in the northern CCS (e.g., Batchelder et al. 2002). While extremely valuable, these observational studies are still very limited by sparsely sampled ecological fields, few ENSO events, and an energetic mesoscale eddy field that together can obscure the signals and decrease their significance levels.

These previous studies generally show reductions of nutrient and plankton levels during warm ENSO events and enhancements for cold ENSO conditions (e.g., Bograd and Lynn 2001; Chávez et al. 2002; Jacox et al. 2016), with indications that El Niño drives the ecosystem toward more subtropical, and fewer subarctic, species components (Mackas and Galbraith 2002; Fisher et al. 2015; Lilly and Ohman 2018, 2021) and favors smaller size-class representation in the web food (Harris et al. 2009; see also Iriarte and González 2004). The signature of ENSO in the CCS has also been found to be asymmetric in the sense that the warm El Niño composite response is weaker, and less significant, than the cool La Niña composite response (Fiedler and Mantua 2017; Turi et al. 2018; Cordero-Quirós et al. 2019). It remains unclear, however, what specific mechanisms are involved in linking the physical and ecological response, how trophic level interactions are modulated, and whether there is sufficient forecast skill (or reproducibility) in the local CCS physical and biological response to ENSO events for practical use (Capotondi et al. 2019; Jacox et al. 2020). Our understanding therefore remains limited regarding how consistently these interannual, and potentially predictable, events drive both the physical and ecological state of this region (see, e.g., Di Lorenzo and Miller 2017; Jacox et al. 2019).

Many previous studies have also used numerical models of the CCS to address these ENSO signals (e.g.,

Curchitser et al. 2005; Frischknecht et al. 2015, 2017; Turi et al. 2018; Cordero-Quirós et al. 2019). Comparing the responses of models with differing levels of complexity (in both physics and ecology) among themselves and with the limited observational basis can give us clearer insight into the possible range of responses, and possible levels of predictive skill, to expect for an ENSO event in the CCS (e.g., Jacox et al. 2019). In general, the large-scale changes associated with ENSO can be well represented by global "coarse-resolution" (~ 100 km) models although these types of models tend to exhibit large biases in representing the finer-scale dynamics of the EBUS (e.g., Van Oostende et al. 2018; Cordero-Quirós et al. 2019). High-resolution, "eddy-scale" (~ 10 km) regional physical-biogeochemical-ecological models are much more appropriate for unravelling the complicated dynamics of upwelling systems like the CCS (e.g., Marchesiello et al. 2003; Di Lorenzo, et al 2005; Gruber et al. 2011; Miller et al. 2015; Frischknecht et al. 2015, 2017, 2018).

In previous work, we considered the ENSO-forced CCS ecological response in a coarse-resolution climate model (Cordero-Quirós et al. 2019). The physical-biological anomalies in that simulation exhibited large-scale coherent relationships related to reduce nutrient and plankton concentrations during El Niño and the reverse during La Niña. However, we found that the anomalous model response in temperature, chlorophyll, and zooplankton was generally much weaker than observed and included other unrealistic features associated with the coarse resolution. In addition, the simplified ecological model only contained a single zooplankton functional group, which limited the capacity of the model ecology to separate ENSO response among the three size classes of phytoplankton.

In this study, we examine the physical-biological response in the California Current to ENSO variability using a high-resolution, "eddy-scale" ocean model that is forced with observed winds. The high (~ 7 km) resolution here now allows proper representation of upwelling fronts along the irregular US West Coast as well as the generation of an energetic and unstable mesoscale eddy field over realistic topography (e.g., Marchesiello et al. 2003; Frischknecht et al. 2015). Additionally, the ecological model here includes two size classes of phytoplankton and three size classes of zooplankton (Kishi et al. 2007; Rose et al. 2015), which is a more realistic representation of potential trophic level interactions than was possible with the single size-class model of zooplankton ENSO response considered by Cordero-Quirós et al. (2019).

The basic state of the spatial distributions of phytoplankton communities, and the dependent zooplankton communities that feed on them and each other, establishes biogeographical regions across and along the CCS in the presence of complicated coastline variations and inhomogeneous

eddy fields (e.g., Venrick 2009; Goebel et al. 2013). We consider here how the simulated local physical and ecological response of the CCS is perturbed by ENSO forcing in this high-resolution, eddy-permitting context. We focus on individually analyzing the two phytoplankton groups and three zooplankton groups to provide a more fine-scaled view of the bottom-up response of the California Current Ecosystem (CCE; e.g., Ohman et al. 2013) to ENSO than is possible with less sophisticated ecological and coarser resolution models (e.g., Franks et al. 2013).

We first address the question of whether a consistent, statistically significant, composite physical-biological response to ENSO events occurs in this eddying model with realistic coastal geometry and bathymetry. We next address whether this model exhibits non-symmetric responses for cold, compared to warm, ENSO events in a similar fashion to those identified in previous analyses. We finally explore whether the trophic levels and size classes of the ecological response follows the physical response in synchrony or whether the response exhibits size-class preferences during warm vs. cold ENSO events. The results reveal coherent physical-ecological responses for both warm and cold events, in spite of the mesoscale eddy "noise," as well as some interesting features of trophic level interactions in the ecology.

We first explain the basic framework of the physical and ecological models along with specification of our observational datasets. Then we introduce our methods for statistically analyzing the system. We follow that with a presentation of results and a discussion and conclusion section.

2 Model framework

2.1 Regional ocean circulation model

The physical fields used for this analysis are from a version of the Regional Ocean Modeling System from Rutgers University (ROMS; Curchitser et al. 2005; Haidvogel et al. 2008; Shchepetkin and McWilliams 2005) in which the physical model is run simultaneously with an ecological model. The study domain spans the zonal extent of the CCS, roughly 1200 km offshore, from Vancouver Island (50° N) to southern Baja California (20° N), over a grid with 1/15° (~7 km) horizontal resolution (Van Oostende et al. 2018). The air-sea fluxes are computed using the Coordinated Ocean-Ice Reference Experiment (CORE; Griffies et al. 2009) protocol using observed reanalysis 6-hourly fields from 1958 to 2007 for the atmospheric variables and model SST. Boundary and initial conditions for temperature, salinity, and velocity are monthly values from the Simple Ocean Data Assimilation (SODA) model output (version 2.1.6), and atmospheric forcing is from the Modern Era Retrospective Analysis for Research and Applications

(MERRA) reanalysis products (Van Oostende et al. 2018). Vertical mixing of momentum and tracers is performed along a vertical grid of 50 terrain-following surfaces (Van Oostende et al. 2018). After dropping 1958 as a "spin-up" year, daily model fields were averaged into monthly means for all model variables for the model time period from January 1959 to December 2007. Climatological monthly mean averages were then formed and subtracted from the monthly means to obtain 1959–2007 monthly anomalies.

2.2 Ecosystem model

The ecological model is called NEMURO (North Pacific Ecosystem Model for Understanding Regional Oceanography; Kishi et al. 2007) and is identical to the ecological model discussed by Politikos et al. (2017) and Nishikawa et al. (2019). NEMURO was developed by PICES CCCC (North Pacific Marine Science Organization, Climate Change and Carrying Capacity Program) as a prototype model to represent the basic trophic structure of the marine ecosystem components in the North Pacific. This lower trophic level nutrient-phytoplankton-zooplankton-detritus (NPZD) model has eleven state variables: nitrate (NO_3), ammonium (NH_4), small phytoplankton (PS), large phytoplankton (PL), small zooplankton (ZS), large zooplankton (ZL), predatory zooplankton (ZP), silicic acid ($Si(OH)_4$), and three detrital pools represented by dissolved organic nitrogen (DON), particulate organic nitrogen (PON), and particulate organic silicate (Opal). The PS and PL groups use parameters that represent flagellates and diatoms, respectively. ZP uses parameters that correspond to euphausiids (or krill) that feed on the mesozooplankton group ZL (parameters for copepods), the microzooplankton group ZS (parameters for ciliates), as well as diatoms (PL). The copepods feed on both the diatoms (PL) and the flagellates (PS) as well as the ciliates (ZS). The ciliates (ZS) feed only on the flagellates (PS). NEMURO uses nitrogen as its primary "currency," but also includes silicon as a limiting nutrient for diatoms. All the state variables are tracked in units of mmol N m^{-3}. The full details and balance equations of NEMURO are given by Kishi et al. (2007), with additional specific parameter information given by Politikos et al. (2017) and Nishikawa et al. (2019).

2.3 Observational benchmark data

The model sea surface temperature anomaly (SSTa) fields were validated and compared with observations from the Hadley Centre Ice-Sea Surface Temperature (HadISST; Rayner et al. 2003) using the time period from January 1959 to December 2007. The model phytoplankton biomass was compared with observed chlorophyll data that was assembled from the Sea-viewing Wide Field-of-view Sensor

(SeaWiFS) Level 3 standard mapped image (SMI), with monthly sampling and 9.2-km resolution (O'Reilly et al. 2000), available only over the model-run overlapping time interval of 1997–2007. The model surface phytoplankton fields were used as a proxy to compare with the satellite chlorophyll fields that sample only over the local oceanic optical depth. Vertical profiles of model NO_3 were compared with observed NO_3 from CalCOFI (Gallo et al. 2019), which is only available for the model-run overlapping 1984–2007 time period at standard CalCOFI levels and stations.

3 Composite analysis and correlation analysis methods

In order to isolate the ENSO signal and remove the impact of long-term trends and decadal climate variability, monthly mean anomalies for all ROMS fields were first high-pass filtered using a Lanczos method with a cut-off frequency of 10 years, following Cordero-Quirós et al. (2019). Identification of El Niño and La Niña years then follows the NOAA protocol for Oceanic Niño Index (ONI) (NCEP/NOAA, http://origin.cpc.ncep.noaa.gov/products/analysis_monitoring/ensostuff/ONI_v5.php), but only includes the moderate-to-strong events and excludes the weak events. In brief, we identify El Niño years as those when Niño-3.4 3-month averaged SSTa ≥ 1.0 °C and La Niña years as those when SSTa ≤ -1.0 °C, where the anomalies persist during both the fall (SON) and winter (DJF) seasons. Since atmospheric teleconnections from the tropics to the mid-latitudes peak in winter for ENSO events, we computed 12-month composites that start in fall (September) before the ENSO peak and end in summer (August) after the peak. This follows the same protocol as Cordero-Quirós et al. (2019).

The resulting years from the ROMS-NEMURO simulation time period included in the 12-month El Niño composite are as follows: 1963–1964, 1965–1966, 1968–1969, 1972–1973, 1982–1983, 1986–1987, 1987–1988, 1991–1992, 1994–1995, 1997–1998, and 2002–2003. The resulting years for the La Niña composite are as follows: 1970–1971, 1971–1972, 1973–1974, 1975–1976, 1983–1984, 1984–1985, 1988–1989, 1995–1996, 1998–1999, and 1999–2000. That yields a total of 11 El Niño events and 10 La Niña events. The neutral composite includes the twelve calendar months (January through December) from the non-ENSO years 1959, 1960, 1961, 1962, 1967, 1977, 1978, 1980, 1981, 1990, 1993, 2001, 2004, 2005, 2006, and 2007.

All the composite variables were tested for significance using a simple bootstrap test as follows: 100 composites were randomly computed using each variable, which were then compared to the actual composites for El Niño and La Niña. Only when anomalies exceeded two standard deviations (2σ) of the random distribution (assumed to be Gaussian) were they considered to be statistically significant at the 95% level using Student's t values. Those grid locations where the composite variability is above this threshold are marked with black dots in the figures.

Additionally, the Pearson's correlation coefficients were computed for the monthly fields in the model using various lags. We focus our analysis here on a 3-month lag of model response with respect to the ONI. This lag was chosen as representative of the whole ecosystem response to ENSO, compared to other similar lags. The 3-month lag is temporally close enough to the peak winter ENSO response in the physical ocean that persistence of those conditions can potentially significantly affect the spring bloom in the ecology. The grid locations where Pearson's correlation is above the 95% significance level are also marked with black dots in the corresponding figures.

Rather than showing all the composite months in the following section, we only focus on key months of the composites and key lag relationships between variables. For this analysis, the nitrate was averaged from 25 to 100 m, which focuses the response on its strongest vertical gradient (nitracline), while the other NPZ model ecological variables were averaged from the surface to 100 m, which includes the full euphotic zone.

4 Results

4.1 SST

The SSTa warming of the CCS associated with El Niño events during winter (DJF 3-month composite average), when the ENSO teleconnections peak, is shown in Fig. 1 for the ROMS simulation and HadISST observations. Composite winter model and observations both show that the warming of the CCS in response to El Niño tends to be significant only along a relatively narrow band along the coast (roughly 300 km) and the warming signal weakens and becomes cool far offshore. Both the model and observations show the most intense warming off the coast of southern Baja California and in the northern portion of the CCS.

Figure 1 also shows the composite DJF SSTa response of the CCS during cold events associated with La Niña. In contrast with El Niño, La Niña is associated with statistically significant cooling over nearly the entire domain of the CCS. The coldest anomalies tend to be at the southern and northern portions of the CCS, comparable to the patterns shown by El Niño-related SSTa, but they extend further offshore where they are consistently cool. This key difference in the consistency of the offshore response to El Niño and La Niña that was identified in previous studies is not strongly affected by the introduction of mesoscale activity.

Fig. 1 Composite DJF average of SSTa for El Niño years (**a,b**) and La Niña years (**c,d**) for both ROMS and HadISST observations as indicated on the top right. The locations where the composite anomalies exceed the 95% significance threshold are marked with black dots

Composite DJF-SSTa
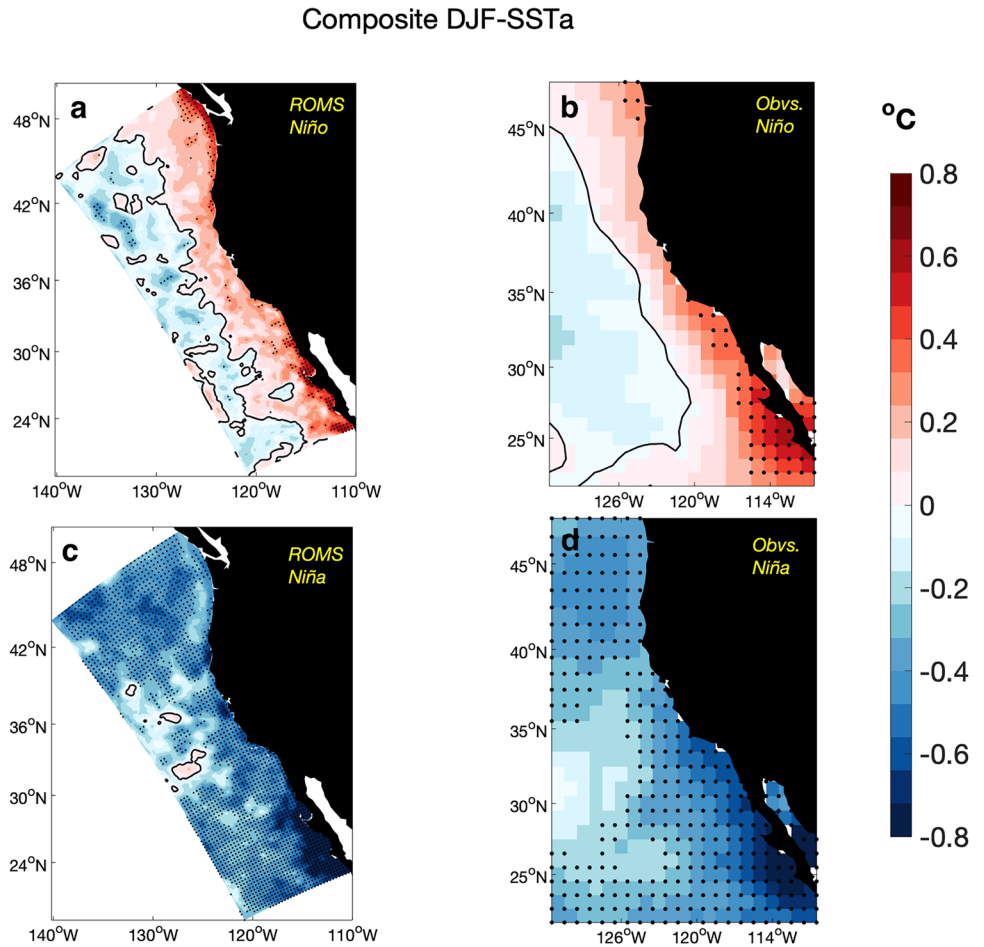
We next further examine the asymmetry between warm and cold events in this simulation. Figure 2 shows the histograms of monthly mean SSTa averaged over the entire model domain as captured by the ROMS and observations during the 12-month composite period from September through August for warm, cold, and neutral ENSO conditions. The histograms show that in the model (Fig. 2, left), the SSTa during neutral and El Niño years tend to be relatively symmetric around the origin so that cold anomalies also frequently occur during El Niño (only 57% of the SSTa are positive during warm events). In contrast, the histogram of model SSTa during La Niña shows a more consistent cooling of the CCS during those years, with less frequent occurrences of warm months (67% of SSTa are cold). Observations are generally consistent with the asymmetry of the model histograms, with 55% of El Niño event anomalies being warm and 64% of the La Niña anomalies being cool. But observations also exhibit stronger anomalies in the histograms. For example, observed neutral years appear to be strongly "tailed" towards warm events, a feature that is not captured by the model.

4.2 Lower trophic level response

We next explored the relationship of the nutrients, phytoplankton, and zooplankton fields to the changes in ENSO conditions. Nitrate and small phytoplankton show a coherent response in winter, but all of the ecological fields showed their largest and most significant ENSO response in the spring (March through May) season when the seasonal phytoplankton bloom occurs. This is in contrast with the physical response that peaks significantly in late winter after the atmospheric teleconnection forcing has generated its largest oceanic signal. Rather than showing the composite maps of all the ecological variability, for brevity, we first show the map for JFM 3-month composite average anomalies of nitrate (which is also structurally representative of the spring) and then present the lagged correlation between the wintertime ENSO index (ONI) and the springtime ecological response. The structures seen in these correlation maps are very similar to those seen in the various composite maps, which are remarkably persistent from month to month in the spring.
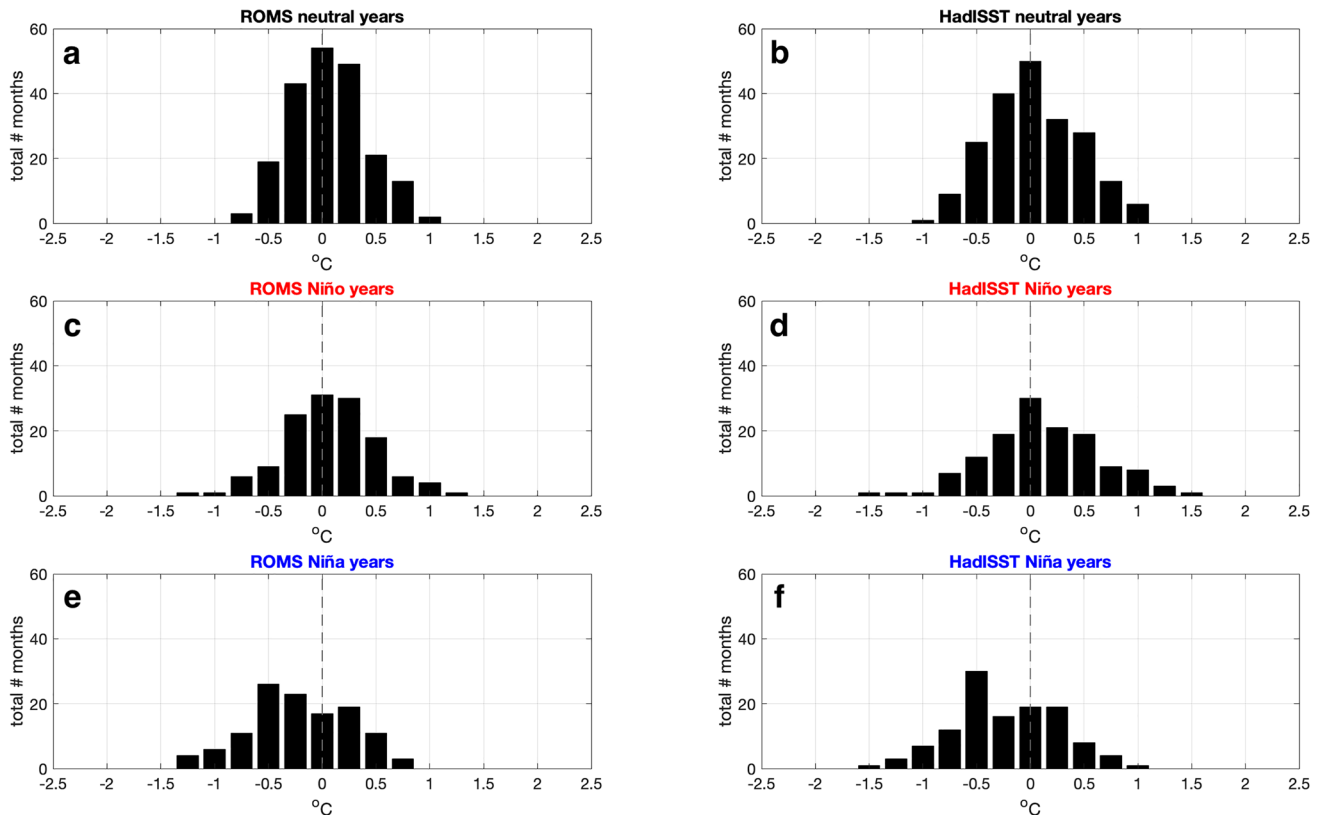
Histograms of SSTa

Fig. 2 Histograms of modeled (**a,c,e**) and observed (**b,d,f**) SSTa during a 12-month period from September through August over the CCS for neutral, El Niño, and La Niña years

4.3 Composite variability of NO₃

The biogeochemical response of the CCS during warm and cold events is succinctly represented by composite anomalies of nitrate (NO_3) concentrations in the water column (averaged from 25 to 100 m) during JFM. Similar results hold for the silicate field (not shown). Figure 3 shows that the composite vertically averaged anomalies of NO_3 in the model captures the nutrient depleted conditions along the coast due to muted coastal upwelling or strengthened downwelling during El Niño and nutrient enhancement due to stronger upwelling during La Niña. The spatial distribution of ENSO-related composite NO_3 anomalies is confined to a roughly 300-km region along the coast, with patchy structures offshore during both warm and cold events. Additionally, anomalies of NO_3 seem to exhibit an undulating pattern of preferred locations of maximum signals along the West Coast.

As a benchmark model validation with limited nitrate observations, we compared model NO_3 vertical profiles from the surface down to 200 m with NO_3 data from CalCOFI for the overlapping time period 1983–2007. The observations

and model nitrate fields were averaged at each of the standard depth levels over a set of 15 stations (line/station: 76.7/49,51,55,60; 80/51,55,60; 81.8/46,46.9; 83.3/51,55,60; and 86.7/45,50,55) near the Santa Barbara coast where the observed nitrate shows a coherent response to forcing by upwelling (Goericke, private communication, 2021), and the model composite NO_3 signal is significant as well.

The vertical profiles in Fig. 4 show these area-averaged composite NO_3 during the spring season (March–April–May) of 5 El Niño years (1987, 1988, 1992, 1995, and 1998) and 5 La Niña years (1984, 1985, 1989, 1996, and 1999) for both the model (diamond line) and observations (dotted line). The model composite exhibits a small low bias in NO_3 during El Niño events, but has comparable NO_3 values to observed La Niña events. The NO_3 concentrations from the model also exhibit somewhat smaller standard deviations (continuous line) for both El Niño and La Niña compared to observations near the surface, but smaller than observations at depth. However, the nutrient enhancement in the composite response to intensified upwelling during La Niña compared to El Niño is clear in both model results and data from CalCOFI, especially in the mid-depths.
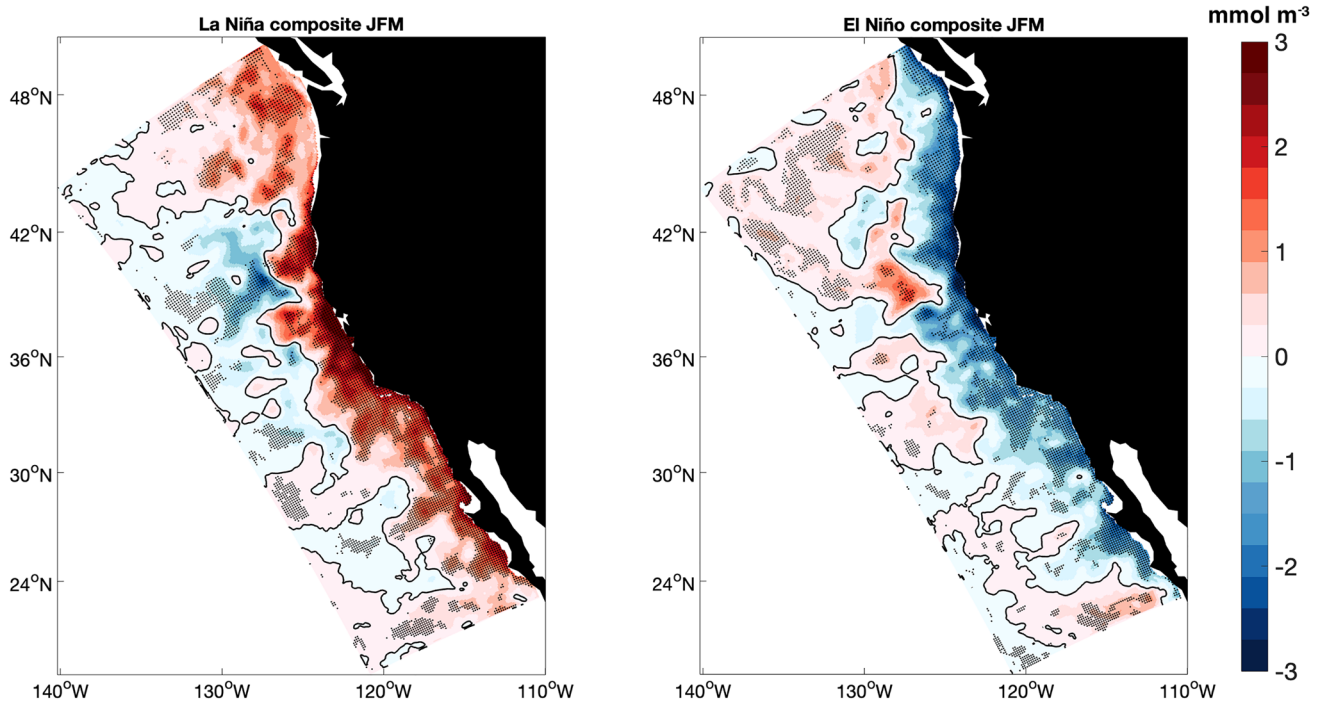
Fig. 3 Composite JFM-averaged anomalies of vertically averaged (25 to 100 m) NO$_3$ for El Niño (left) and La Niña (right) years. Locations where the composite response exceeds the 95% significance threshold are marked every 5 grid points (black dots)

Fig. 4 Composite spring (MAM) vertical profiles (solid lines) of NO$_3$ during El Niño (left) and La Niña (right) for both model and CalCOFI averaged over the near-coastal area defined by CalCOFI lines 76.7, 80, 81.8, 83.3, and 86.7 off Santa Barbara coast. Standard deviation for both model and observations are indicated by the shaded area between the dashed lines
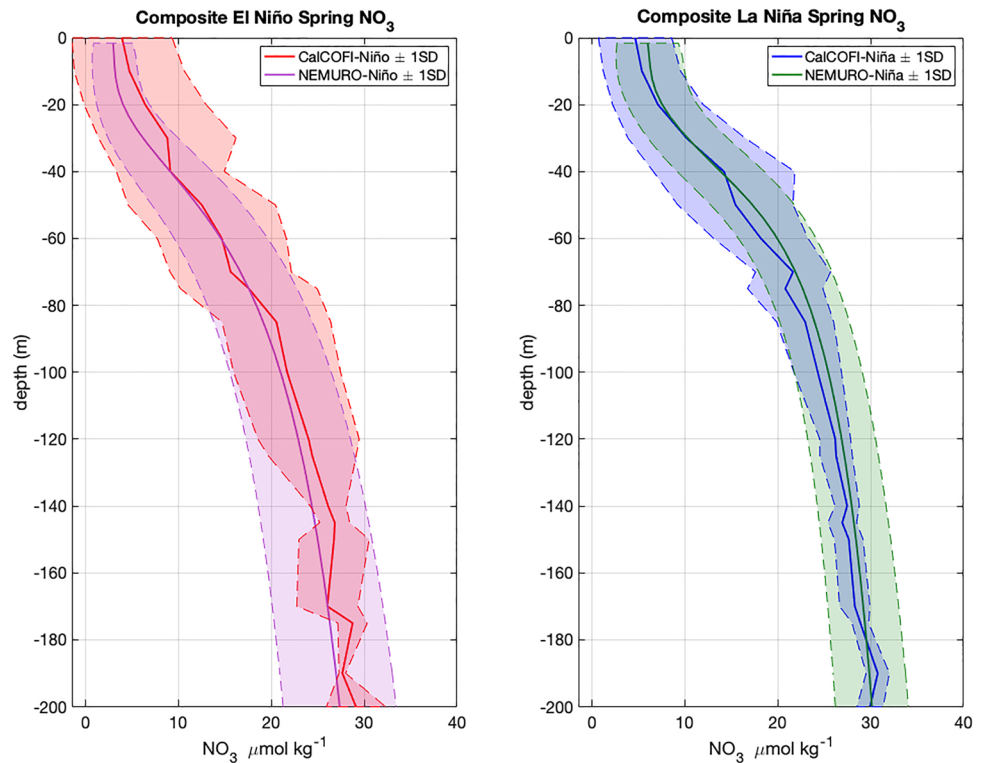
4.4 Lagged correlation of lower trophic levels with the ONI

Figure 5 shows the 3-month lagged correlation between January ONI values and April anomalies of the ecological fields in NEMURO. April was selected as a representative month of peak upwelling and related ecological response, although peak upwelling is dependent on latitude in the CCS (García-Reyes and Largier 2012; Jacox et al 2018; Boldt et al. 2020). Positive values (red) indicate that biomass anomalies during April over the CCS are in phase with the SSTa in January over the tropical Pacific. During El Niño conditions over the CCS, when upwelling favorable winds tend to be weaker, the nutrient supply to the photic zone decreases, as shown by the negative lagged-correlations of vertically averaged NO_3 (which is similar to the silicate fields) along the coastal region. As a consequence of the nutrient-depleted waters, large phytoplankton (diatoms, Fig. 5c) biomass decreases along the coastal band and in patchy areas offshore. The response of the predatory zooplankton (krill, Fig. 5f) and mesozooplankton (copepods, Fig. 5e), which each graze partly on diatoms, resembles this diatom field. The predatory zooplankton has a stronger correlative response to ONI

than mesozooplankton since it preys upon the now-reduced field of mesozooplankton. Thus, the larger components of the model food web respond as anticipated with reductions in biomass for El Niño conditions and enhancements for La Niña conditions.

In contrast, Fig. 5 shows that positive anomalies of small phytoplankton (flagellates, Fig. 5b) biomass occur during warm event conditions (positive ONI) along the coastal region. Small zooplankton (ciliates, Fig. 5d) also increases in these near-coastal areas, consistent with the enhancement of its only model food source (the flagellates) and with the reductions in both of its predators (euphausiids and copepods). Thus, the small components of the food web respond with increases in biomass for El Niño conditions and reductions for La Niña conditions.

As a benchmark model validation with limited chlorophyll observations, we compared model phytoplankton biomass and satellite chlorophyll data over the overlapping time interval of 1997–2007. These fields were averaged along the coastal band from 32° to 42° N, extending 100 km offshore, where both the composite model response to ENSO of diatoms and nanophytoplankton is the most coherent and the very high chlorophyll values that are very close to the coast
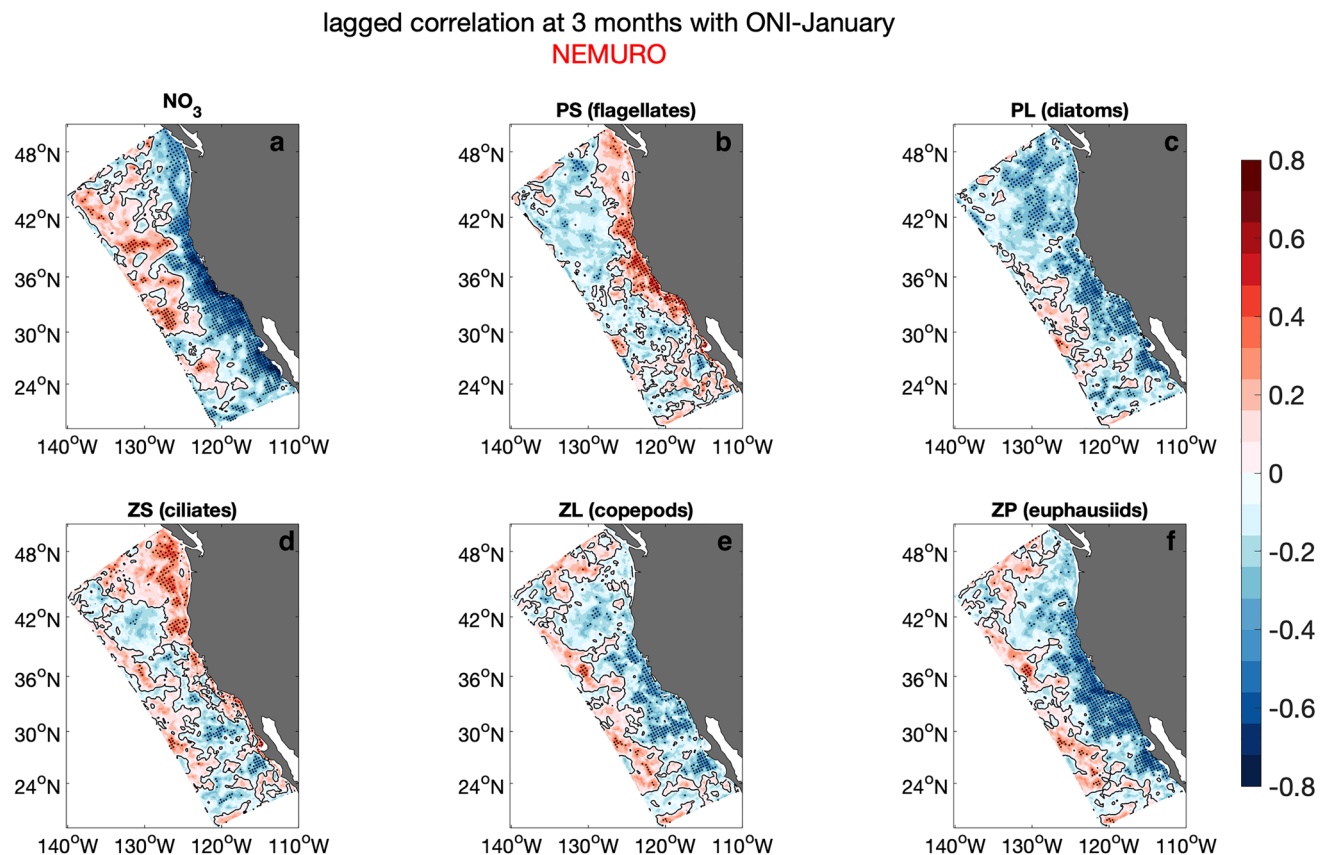

Fig. 5 Lagged correlation of ecological fields during April with January of the Oceanic Niño Index (ONI). Locations where correlations are > 95% confidence level are marked with black dots

occur in observations (Henson and Thomas 2007). Figure 6a shows the monthly means (including the seasonal cycle) in this area of the model phytoplankton biomass (black line), i.e., the sum of diatom and nanophytoplankton biomass at the surface, and observed surface chlorophyll concentrations from satellite data (green line). The model seasonal cycle exhibits higher year-to-year and season-to-season variability than the observations, but the timing of the spring bloom is consistent with that of observations. There are too few warm and cold events in this overlapping time interval to construct a reliable composite ENSO response, but the increase in chlorophyll/phytoplankton during the 1997–1998 to 1999 warm-to-cold transition is evident in both model and observation. Figure 6b (bottom) shows the anomalies of the two model phytoplankton size classes separately, with spring months (MAM) circled in red for 2 El Niño years (1998, 2003) and 2 La Niña years (1999, 2000) in blue. The generally out-of-phase relationship of these biomass anomalies seen in this time series of the model anomalies is consistent with the results shown in Fig. 5b and c, where nanophytoplankton biomass increases during low-nutrient El Niño warm conditions while diatom biomass decreases and vice versa. Note, however, that the magnitude of the nanoplankton biomass anomalies is only roughly 3% of the magnitude of the diatom biomass anomalies, which is consistent with the relative size of their total biomass.

An interesting feature of the model ecological correlation spatial maps is the occurrence of significant ecological anomalies locked spatially to the same locations along the coast in the simulated California Current (Fig. 5). Figure 7 shows the mean sea-level height field over the entire period of our simulation. Large-scale standing eddies (roughly four
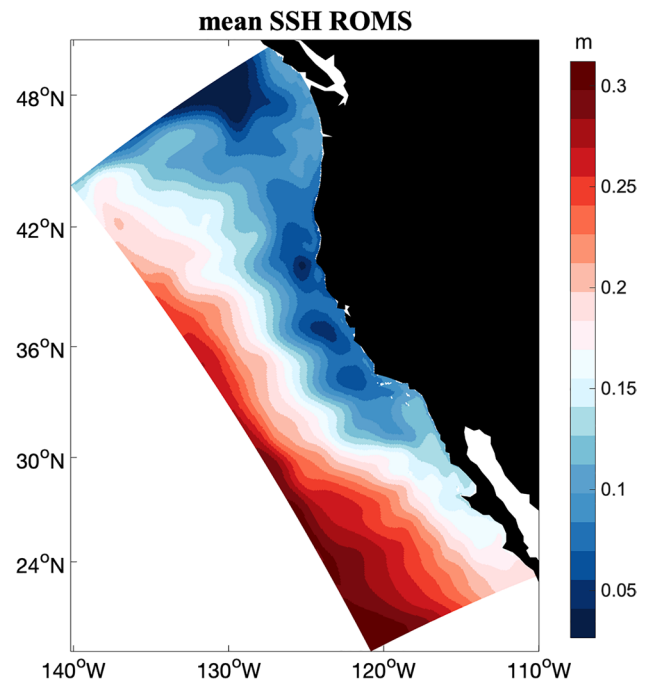

Fig. 7 Long-term mean of sea surface height (SSH) from the ROMS monthly fields from 1959 to 2007

to five of them, undulating north–south along the CCS) are climatologically locked to major capes and bathymetric features. These climatological stationary-wave, eddy features are visually associated with the alongshore local ecological mesoscale response patterns seen in Fig. 3 and the alongshore mesoscale distribution of composite NO_3 anomalies in Fig. 2.

Fig. 6 **a** Time series of model (black) phytoplankton biomass (mmol N m^{-3}) and satellite observations (green) of surface chlorophyll (mg m^{-3}) data averaged over a 100-km coastal band extending from San Diego to Oregon (32° to 42° N). **b** Surface anomalies of nanophytoplankton and diatom biomass from the model averaged over the same area. Red circles indicating MAM months for El Niño years: 1998 and 2003; blue circles indicating MAM months for La Niña years: 1999 and 2000
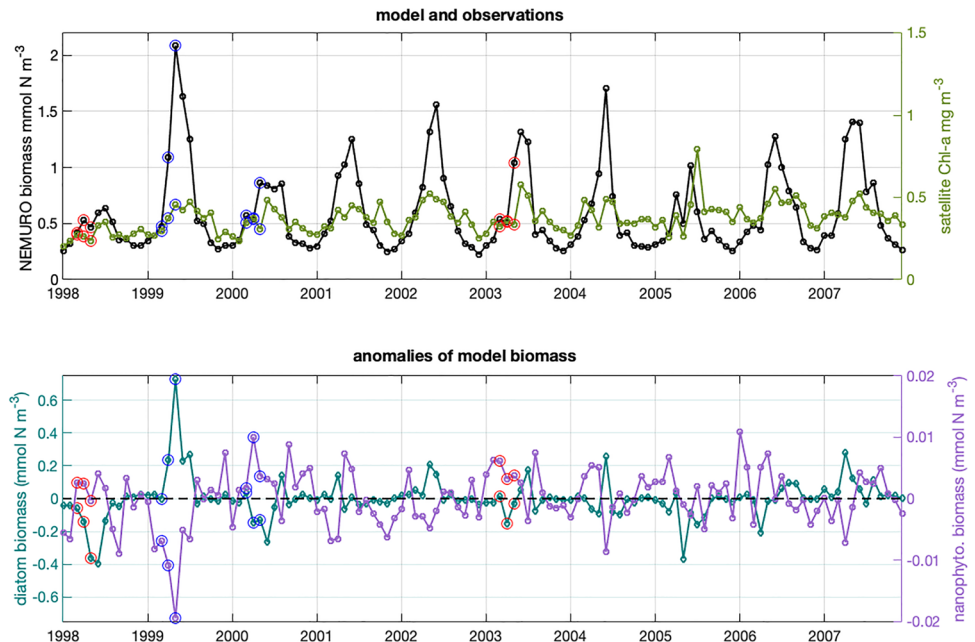
We looked with more detail into the structure of the mesoscale eddy response of the CCS in ROMS by analyzing composites of sea surface height anomalies (SSHa) during winter for El Niño and La Niña events. Figure 8 shows that a consistent rise in sea level occurs during El Niño and a consistent lowering of sea level occurs during La Niña all along the coastal region of the CCS. This implies a large-scale weakening of the surface California Current during El Niño and a strengthening of the surface current during La Niña. But the eddy structures in the SSHa do not line up with mesoscale structures seen in the ecological response in Fig. 4 or seen in the nitrate composite in Fig. 2. This is consistent with the results of the modeling study of Fiechter et al. (2018) who showed that local ecological response can be modulated by the alongshore meanders in the geostrophic circulation, and not necessarily locked to capes or bathymetric features.

4.5 Probability distribution of ecological fields over the CCS

In order to address differences in the consistency of the ecological response of the CCE to warm and cold ENSO events, we computed histograms of the ecological fields in NEMURO over a coastal swath from 22° to 48° N extending roughly 300 km offshore, which is the region

of strongest response to ENSO seen in the composites (Figs. 9–10). The percentage of cold and warm anomalies associated to each event for each ecological group and SST are summarized in Table 1. The histograms of NO_3 anomalies show a fairly consistent depletion during El Niño years with fairly consistent enhancement of NO_3 during La Niña (Fig. 9). Negative anomalies represent 71% of the total distribution for El Niño years, and 77% of the anomalies are positive for La Niña years, which is a much more symmetric response than found for the SSTa histograms (Fig. 2).

Histograms for diatoms, in contrast, have more consistency during cold events, with 70% positive anomalies during La Niña and 59% negative anomalies during El Niño (Fig. 9). The ciliates, however, are less consistently altered (Fig. 10) than diatoms for both warm (49%) and cold events (57%), possibly due to our selected averaging area that is not aligned with their narrower coastal response and their higher signals in high latitudes (see Fig. 5). The distribution for predatory zooplankton (Fig. 10) is less consistent than for diatoms, with El Niño (La Niña) events having 64% (70%) of their associated anomalies on the negative (positive) side of the distribution. Similar results hold for the copepod distributions (50% vs. 69%). Additionally, the ciliates reflect the flagellate distribution (47% vs. 63%) but with a stronger consistency during La Niña events.
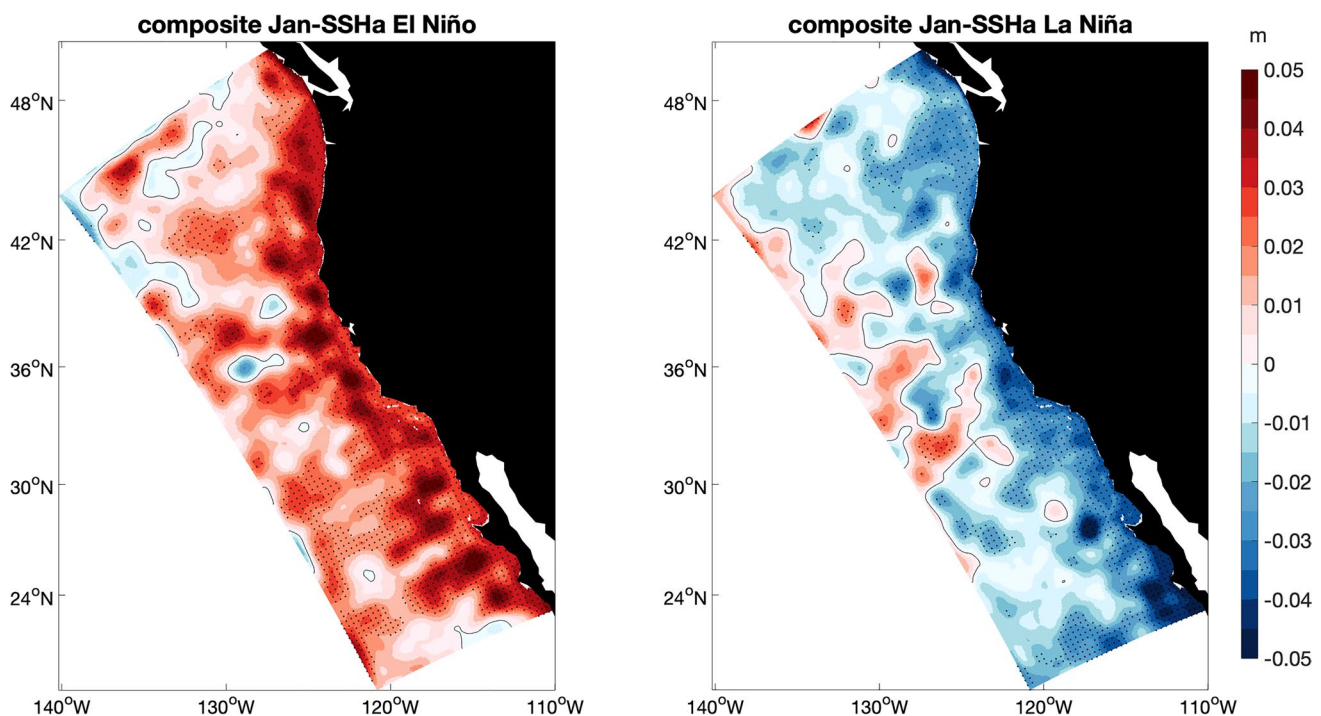

Fig. 8 Composite January anomalies of the ROMS sea surface height (SSHa) for El Niño (left) and La Niña (right) events. Locations where the composite anomalies exceed the 95% significance threshold are marked with black dots
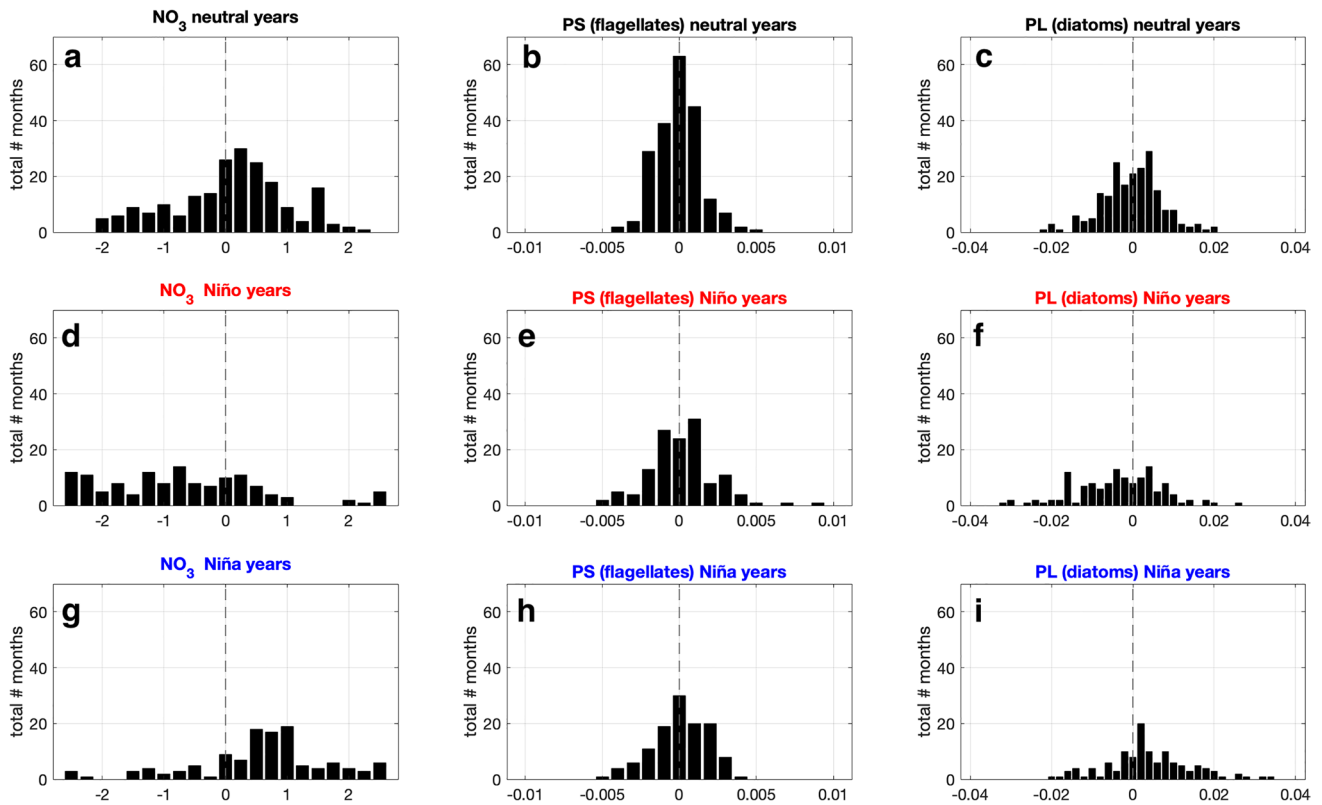
Ecological histograms-NEMURO

Fig. 9 Histograms of anomalies of vertically averaged NO$_3$, biomass of small phytoplankton, and diatoms, during a 12-month period from September through August over a coastal swath of ~ 300 km off-shore from 22° to 48° N. Anomalies are shown for neutral years (**a,b,c**), El Niño (**d,e,f**), and La Niña (**g,h,i**) and are expressed in units of mmol N m^{-3}

5 Discussion and conclusion

We analyzed the bottom-up ENSO-driven physical-biological response of the CCS and the CCE in a high-resolution, "eddy-scale" ocean model with two classes of phytoplankton and three classes of zooplankton. We used a statistical analysis strategy involving composites, lag correlations, and histograms to assess the ENSO-forced physical, biogeochemical, and ecological response. Observations of SST, satellite chlorophyll, and subsurface nitrate revealed some small biases in the model response, but generally corroborated the model behavior. The near-coastal signature of the various model responses suggests that the response to El Niño is tightly linked to the coastal dynamics controlled by the weakening of the upwelling winds during El Niño that lead to muted upwelling and consequent warming of the coastal SSTa.

The asymmetry in SSTa between CCS warm and cold ENSO events that was seen in observations by Fielder and Mantua (2017), the 10-km-resolution model of Turi et al. (2018), and the 100-km coarse resolution model of Cordero-Quirós et al. (2019), also occurs in this 7 km-resolution simulation (Figs. 1–2). Overall, these results further confirm the

asymmetrical response of the CCS in which La Niña events are associated with a more consistent, and broader-scale, cooling than El Niño events are associated with consistent warming, even though El Niño is associated with the most extreme (warm) SSTa events (e.g., McGowan et al. 1998). This key difference in the consistency of the response to El Niño and La Niña is not strongly affected by the introduction of mesoscale activity, indicating that its origin lies in the large-scale dynamical ocean response to atmospheric forcing. The most extreme model SST anomalies, however, tended to be weaker than some of the observed warm extremes, which may be due to model biases, the mismatch of air–sea coupling on the eddy scale due to the forcing protocol (e.g., Seo et al. 2016), or simply due to the random mesoscale activity that occurs differently in the model and observations.

In general, the histograms of all the biological fields (nutrient, phytoplankton, zooplankton; Figs. 9–10, Table 1) in NEMURO do not exhibit as strong of an asymmetry as that associated with SSTa (Fig. 2, Table 1). For example, the composite anomalies of NO$_3$ are quite symmetric (Fig. 3) over the CCS in both in their spatial pattern and significance,

Ecological histograms-NEMURO
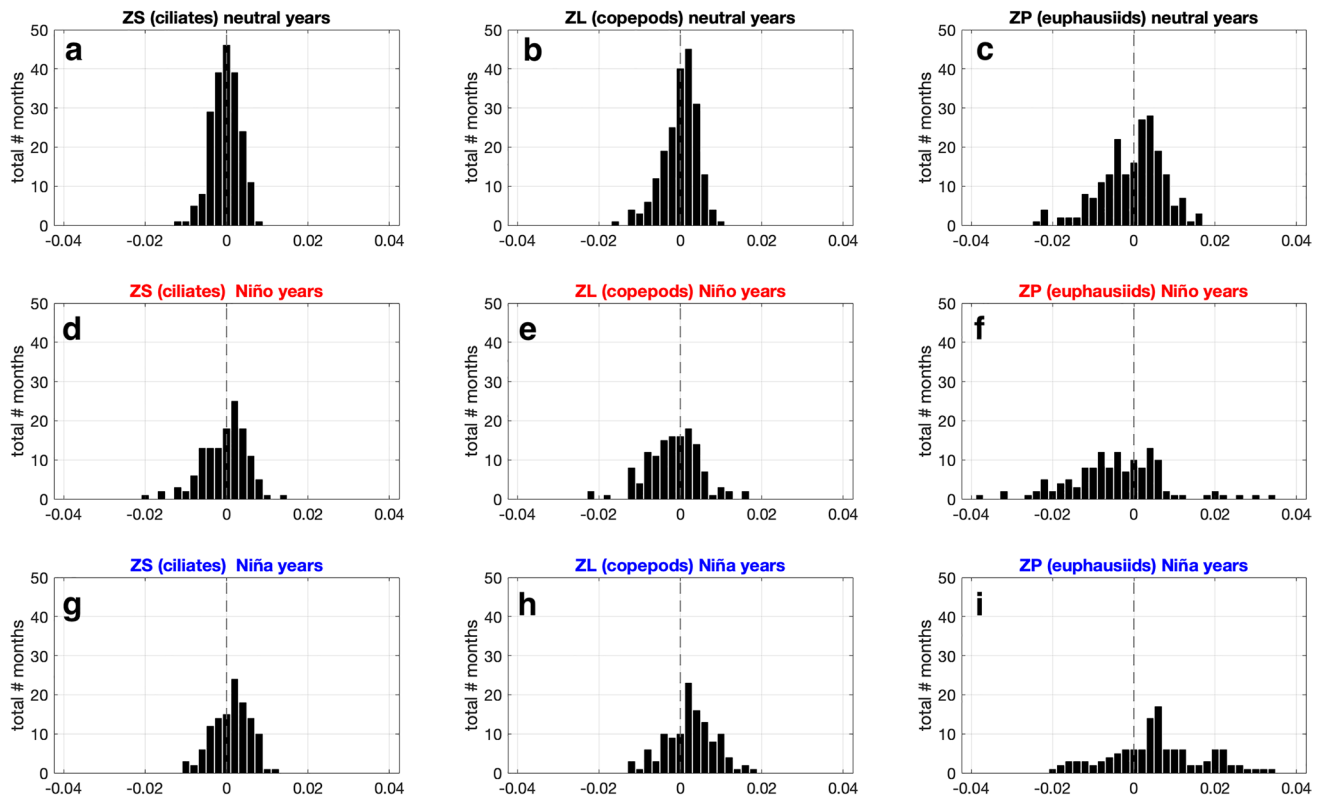### zooplankton groups

Fig. 10 Histograms of anomalies of biomass for small zooplankton, large zooplankton, and predatory zooplankton during a 12-month period from September through August over a coastal swath of ~300 km off-shore from 22° N to 48° N. Anomalies are shown for neutral years (**a,b,c**), El Niño (**d,e,f**), and La Niña (**g,h,i**) and are expressed in units of mmol N m^{-3}

Table 1 Percentage of negative anomalies during El Niño years (second column) and positive anomalies during La Niña years (last column) for ecological variables. Likewise, for percentage of positive anomalies for SSTa in model and observations

	EN < 0 (%)	LN > 0 (%)
NO$_3$	71	77
PS	49	57
PL	59	70
ZS	47	63
ZL	58	69
ZP	64	70
SST ROMS	57	67
SST HadISST	55	64

especially for the central CCS. The spatial distribution of ENSO-related composite NO$_3$ anomalies is confined to a roughly 300-km region along the coast, with more patchy structure offshore during both warm and cold events. This supports the interpretation of an upwelling-driven response of the NO$_3$ to large-scale wind changes. Changes in the biogeochemistry of the source waters (e.g., Rykaczewski and

Dunne 2010; Bograd et al. 2015) and the advection fields (e.g., Lilly et al., 2018) may also partly affect these nutrient loading patterns, but identifying those subsurface influences would require additional experiments such as with passive tracers (e.g., Combes et al. 2013) or the use of an adjoint model (e.g., Song et al. 2011, 2012).

We found that the larger ecological components (diatoms, euphausiids, and copepods) are suppressed in the coastal upwelling zones during El Niño, while the smaller components (flagellates and ciliates) are enhanced. That the larger components of the simulated food web respond with reductions in biomass for El Niño conditions and enhancements for La Niña conditions are expected from many previous studies. But the enhancement of the biomass of small components of the food web during El Niño was not anticipated, although previous observational studies have hinted at this effect (e.g., Harris et al. (2009) for the warm-to-cold transition around the 1997–1998 El Niño off Vancouver Island; Iriarte and González (2004) for the response off the northern coast of Chile during the 1997–1998 El Niño). The response of the small phytoplankton is consistent with their cells having lower nutrient requirements and more effective uptake,

which gives them competitive advantage over larger cells (diatoms) under low nutrient conditions (Van Oostende et al. 2018; Edwards et al. 2012). Figure 5 clearly shows that NEMURO captures the kind of ecosystem dynamics where the smaller phytoplankton groups thrive under lower nutrient conditions nearshore due to muted upwelling during El Niño. This "El Niño winners and losers" characteristic is a noteworthy result of our analysis of this simulation with multiple classes of phytoplankton and zooplankton and shows the efficacy of adding more complexity to the food web compared to more simplistic ecological models.

Our ecological model results are largely consistent with the numerous observational studies that report overall reductions in the total biomass of euphausiids and copepods during El Niño-like conditions over the CCS (Bograd and Lynn 2001; Chávez et al. 2002; Mackas and Galbraith 2002; Jacox et al. 2015; Fisher et al. 2015; Lilly and Ohman 2018, 2021). However, most observational studies of the ecological response to ENSO in this region aggregate phytoplankton size classes and zooplankton size classes so that our results cannot be directly compared with them. Some observational studies demonstrate swings from cold water species to warm water species during El Niño (e.g., Fisher et al. 2015; Mackas and Galbraith 2002; Lilly and Ohman 2018, 2021) but our model does not contain species-specific information to allow a direct comparison. Additionally, many observational studies focus on a single (or only a few) El Niño event, which limits statistical reliability. Moreover, when attempting to measure biological fields during cruises, oceanic mesoscale eddies in nature contribute additional noise to the system that limit our ability to establish the significance of response to ENSO. Our composite approach to a modeling study over the 1959–2007 time period is successfully able to identify a consistent and significant response embedded in this energetic mesoscale eddy field.

In general, chlorophyll observed from satellites is often used as a proxy for phytoplankton biomass. This approach facilitates model comparison with satellite observations of chlorophyll (e.g., Thomas et al. 2012), and our model results are reasonably consistent with observations in that context. However, the types of algorithms that are used for chlorophyll computation involve variables that are unique to each phytoplankton size class, e.g., grazing and mortality rates, and saturation constants for nutrient uptakes. Thus, although using chlorophyll as a proxy for phytoplankton biomass may provide an overall broad-brush view of the response of the ecosystem to ENSO, the complexity of its calculation can obscure the interesting ecological dynamics at lower trophic levels.

The dichotomy in the details of the simulated bottom-up response of the CCE to ENSO (Fig. 5) motivates us to identify interactions between the lower trophic levels. When El Niño drives nutrient depletion in the photic zone due to

suppressed upwelling, the larger phytoplankton (diatoms) have less nutrients available for their uptake and growth, resulting in decreased biomass. It is unclear whether the decrease in diatoms biomass is solely a consequence of nutrient limitation or also significantly influenced by mortality and grazing, but future research could analyze the changes in opal detrital pool in order to address this issue. Small phytoplankton are more resilient to nutrient depletion since their size allows for smaller nutrient concentrations and at the same time they face less competition from diatoms for nutrients. During La Niña, intensified upwelling brings nutrients to the photic zones favoring phytoplankton populations, particularly the larger ones with more capacity for uptake. Competition then comes into play, and small phytoplankton concentrations are reduced under upwelling favorable conditions.

We also found that significant anomalies of the ecological model variables (Fig. 5) seem to follow the semi-permanent SLH meanders of the CCS mean state (Fig. 7). These standing eddies (also called permanent meanders or stationary waves) in the simulated California Current have been previously discussed for the physical fields of currents and SLH (Marchesiello et al. 2003; Centurioni et al. 2008) and were linked to the ecological fields modeled by Fiechter et al. (2018) where the geostrophic circulation served as a modulator of the local upwelling. However, we have not noticed any previous published discussion of this type of standing-eddy ecological response modulation being so clearly linked to ENSO. Figure 7 shows the mean sea-level height field over the entire period of our simulation. Its meandering structure is consistent with what was previously found by Centurioni et al. (2008) for a shorter-term mean of the SSH field from ROMS. The large-scale standing eddies (roughly four-to-five of them, undulating north–south along the CCS) are climatologically locked to major capes and bathymetric features and can also be associated with local enhancements of the mesoscale eddy field (not shown for this simulation but discussed previously by Centurioni et al. 2008). The persistent meanders might be channels for filament ejection of biomass from coastal regions, whereby strong production near the coast is transported offshore by the eddies or the mean flow. But it remains unclear how the vigorous mesoscale features of the CCS fundamentally influence the variability of the biogeochemical properties of the CCE and how this further impacts the spatial distribution of phytoplankton and zooplankton communities. A recent study by Chabert et al. (2020) found that offshore patches of high chlorophyll concentrations are consistent with variations of the mesoscale field, measured as changes in total kinetic energy (TKE). Moreover, their results suggest that low levels of TKE are associated with El Niño events, while greater TKE is associated with La Niña. Further research is necessary to establish stronger links between

variability of the mesoscale field and ENSO events, but such results indicate that this topic is worthy of exploration in order to better understand the physical-biogeochemical interactions in the CCS during ENSO conditions.

We further examined the anomalous SLH structures during winter for El Niño and La Niña events and found that they exhibit a large-scale coherent alongshore signal associated with weakening of the surface California Current during El Niño and a strengthening of the surface current during La Niña. This response can be dynamically driven by pycnocline depth changes associated with CCS ENSO anomalies and also enhanced by thermal expansion effects. However, the patterns of ENSO-forced eddy SLH structures in Fig. 8 were not consistently localized around the mean-flow standing eddies of Fig. 7. This suggests that the large-scale forcing from the atmosphere modulates the mean state of the CCS during ENSO events, rather than by consistently changing the local mesoscale eddy dynamics that develop around the persistent meanders in this simulation (e.g., Davis and Di Lorenzo 2015). Additional research is necessary to better elucidate how changing ENSO conditions can modulate the large-scale background flow and affect physical-biological dynamics of the mesoscale eddy field, such as by using ensembles of long simulations that can add more significance to the eddy statistics for repeated occurrences of ENSO events.

In conclusion, the results of this work show that a simple lower trophic level NPZD model like NEMURO is a useful tool to represent the bottom-up ENSO-related response of the CCE in ROMS. The high resolution of the regional circulation model allows for the fundamental effects of mesoscale-eddy and frontal-scale features that drive variability in the CCS. The results help to understand some aspects of the degree of consistency, and thereby predictability, of the CCE that could be used in a practical forecasting sense on seasonal to interannual timescales (e.g., Jacox et al. 2020), as well as in a climate projection sense as we transition into warmer global temperatures on decadal to centennial timescales (e.g., Tommasi et al. 2017; Schmidt et al. 2020). A firm scientific knowledge of the evolution of bottom-up dynamics of the ecosystem as driven by changes in the physical forcings is key to understand future changes in primary production and higher trophic levels (e.g., Overland et al. 2010). Patterns of fish migration highly depend on the regions of high nutrient concentration, and fish catch is strongly related to high chlorophyll coastal regions (Stock et al. 2017). Shedding more light on these dynamics will help us better address the future changes of habitat of fish populations like sardine and anchovy, as well as top predators, as a response of changes in their environmental modulators on seasonal, interannual, and global warming timescales (e.g., Ito et al. 2010; Bakun et al. 2015; Fiechter et al. 2015).

Data availability The observational datasets are all available from the sources cited in the paper. The modeling dataset is available from the authors on reasonable request.

Code availability Not applicable.

Declarations

Conflict of interest The authors declare no competing interests.

References

Alexander MA, Bladé I, Newman M, Lanzante JR, Lau NC, Scott JD (2002) The atmospheric bridge: the influence of ENSO teleconnections on air–sea interaction over the global oceans. J Climate 15:2205–2231

Bakun A, Black BA, Bograd SJ, Garcia-Reyes M, Miller AJ, Rykaczewski RR, Sydeman WJ (2015) Anticipated effects of climate change on coastal upwelling ecosystems. Curr Clim Change Rep 1:85–93

Batchelder HP, Barth JA, Kosro PM, Strub PT, Brodeur RD, Peterson WT, Tynan CT, Ohman MD, Botsford LW, Powell TM, Schwing FB, Ainley DG, Mackas DL, Hickey BM, Ramp SR (2002) The GLOBEC northeast Pacific California Current System program. Oceanography 15:36–47

Bograd SJ, Lynn RJ (2001) Physical-biological coupling in the California Current during the 1997–1998 El Niño-La Niña cycle. Geophys Res Lett 28:275–278

Bograd SJ, Pozo Buil M, Du Lorenzo E, Castro CG, Shroeder ID, Goericke R, Andersson CR, Benitez-Nelson C, Whitney FA (2015) Changes in source waters to the Southern California Bight. Deep Sea Res 112:42–52

Boldt JL, Javorski A, Chandler PC (Eds.) (2020) State of the physical, biological and selected fishery resources of Pacific Canadian marine ecosystems in 2019. Can Tech Rep Fish Aquat Sci 3377: 288 p

Capotondi A, Jacox M, Bowler C, Kavanaugh M, Lehodey P, Barrie D, Brodie S, Chaffron S, Cheng W, Faggiani Dias D, Eveillard D, Guidi L, Iudicone D, Lovenduski N, Nye JA, Ortiz I, Pirhalla DE, Pozo Buil M, Saba V, Sheridan SC, Siedlecki S, Subramanian A, De Vargas C, Di Lorenzo E, Doney SC, Hermann AJ, Joyce T, Merrifield M, Miller AJ, Not F, Pesant S (2019) Observational needs supporting marine ecosystems modeling and forecasting: From the global ocean to regional and coastal systems. Front Mar Sci 6:623

Centurioni LR, Ohlmann JC, Niiler PP (2008) Permanent meanders in the California Current System. J Phys Oceanogr 38:1690–1710

Chabert P, d'Ovidio F, Echevin V, Stukel MR, Ohman MD (2020) Cross-shore flow and implications for carbon export in the California Current Ecosystem: a Lagrangian analysis. J Geophys Res Oceans 126. https://doi.org/10.1029/2020JC016611

Chávez FP, Pennington JT, Castro CG, Ryan JP, Michisaki RP, Schlining B, Walz P, Buck KR, McFadyen A, Collins CA (2002) Biological and chemical consequences of the 1997–1998 El Niño in central California waters. Prog Oceanogr 54:205–232. https://doi.org/10.1016/S0079-6611(02)00050-2

Checkley DM, Barth JA (2009) Patterns and processes in the California Current System. Prog Oceanogr 84:49–64

Combes V, Chenillat F, Di Lorenzo E, Rivière P, Ohmane MD, Bograd SJ (2013) Cross-shore transport variability in the California Current: Ekman upwelling vs. eddy dynamics. Prog Oceanogr 109:78–89

Cordero-Quirós N, Miller AJ, Subramanian AC, Luo JY, Capotondi A (2019) Composite physical-biological El Niño and La Niña conditions in the California Current System in CESM1-POP2-BEC. Ocean Model 142:101439

Curchitser EN, Haidvogel DB, Hermann AJ, Dobbins EL, Powell TM, Kaplan A (2005) Multi-scale modeling of the North Pacific Ocean: assessment and analysis of simulated basin-scale variability (1996–2003). J Geophys Res 110:C11021

Davis A, Di Lorenzo E (2015) Interannual forcing mechanisms of California Current transports II: mesoscale eddies. Deep-Sea Res Part II-Top Stud Oceanography 112:31–41

Di Lorenzo E, Miller AJ, Schneider N, McWilliams JC (2005) The warming of the California Current: dynamics and ecosystem implications. J Phys Oceanogr 35:336–362

Di Lorenzo E, Miller AJ (2017) A framework for ENSO predictability of marine ecosystem drivers along the US West Coast. US CLIVAR Variations 15:1–7

Edwards KF, Thomas MK, Klausmeier CA, Litchman E (2012) Allometric scaling and taxonomic variation in nutrient utilization traits and maximum growth rate of phytoplankton. Limnol Oceanogr 57:554–566

Fiechter J, Rose KA, Curchitser EN, Hedstrom KS (2015) The role of environmental controls in determining sardine and anchovy population cycles in the California Current: analysis of an end-to-end model. Prog Oceanogr 138:381–398

Fiechter J, Edwards CA, Moore AM (2018) Wind, circulation, and topographic effects on alongshore phytoplankton variability in the California Current. Geophys Res Lett 45:3238–3245

Fiedler PC, Mantua NJ (2017) How are warm and cool years in the California Current related to ENSO? J Geophys Res Oceans 122(7):5936–5951. http: //dx.doi.org/10.1002/2017JC013094.

Fisher JL, Peterson WT, Rykaczewski RR (2015) The impact of El Niño events on the pelagic food chain in the northern California Current. Glob Change Biol 21:4401–4414

Franks PJS, Di Lorenzo E, Goebel NL, Chenillat F, Riviere P, Edwards CA, Miller AJ (2013) Modeling physical-biological responses to climate change in the California Current System. Oceanography 26:26–33

Frischknecht M, Munnich M, Gruber N (2015) Remote versus local influence of ENSO on the California Current System. J Geophys Res Oceans 120:1353–1374

Frischknecht M, Münnich M, Gruber N (2017) Local atmospheric forcing driving an unexpected California Current System response during the 2015–2016 El Niño. Geophys Res Lett 44:304–311

Frischknecht M, Münnich M, Gruber N (2018) Origin, transformation, and fate: the three-dimensional biological pump in the California Current System. J Geophys Res Oceans 123:7939–7962

Gallo ND, Drenkard E, Thompson AR, Weber ED, Wilson-Vandenberg D, McClatchie S, Koslow JA, Semmens BX (2019) Bridging from monitoring to solutions-based thinking: lessons from CalCOFI for understanding and adapting to marine climate change impacts. Front Mar Sci 6:695

García-Reyes M, Largier JL (2012) Seasonality of coastal upwelling off central and northern California: new insights, including temporal and spatial variability. J Geophys Res 117:C03028

Goebel NL, Edwards CA, Zehr JP, Follows MJ, Morgan SG (2013) Modeled phytoplankton diversity and productivity in the California Current System. Ecol Model 264:37–47

Griffies S, Biastoch C, Bryan F, Danabasoglu G, Chassignet EP, England MH, Gerdes R, Haak H, Hallber RW, Hazeleger W, Jungclaus J, Large WG, Madec F, Pirani A, Samuels B, Sheinert M, Gupta AS, Severijns CA, Simmons HL, Treguier AM, Winton M, Yeager S, Yin J (2009) Coordinated ocean-ice reference experiments (CORE). Ocean Model 26:1–46

Gruber N, Lackhar Z, Frenzel H, Marchesiello P, Münnich M, McWilliams JC, Nagai T, Plattner G-K (2011) Eddy-induced reduction of biological production in eastern boundary upwelling systems. Nat Geosci 4:787–792. https://doi.org/10.1038/NGEO1273

Haidvogel DB, Arango H, Budgell WP, Cornuelle BD, Curchitser E, DiLorenzo E, Fennel K, Geyer WR, Hermann AJ, Lanerolle L, Levin J, McWilliams JC, Miller AJ, Moore AM, Powell TM, Shchepetkin AF, Sherwood CR, Signell RP, Warner JC, Wilkin J (2008) Regional ocean forecasting in terrain- following coordinates: model formulation and skill assessment. J Comput Phys 227:3595–3624

Harris SL, Varela DE, Whitney FW, Harrison PJ (2009) Nutrient and phytoplankton dynamics off the west coast of Vancouver Island during the 1997/98 ENSO event. Deep Sea Res Part II 56:2487–2502

Henson, S. A., & Thomas, A. C. (2007). Phytoplankton scales of variability in the California Current system: 1. Interannual and cross-shelf variability. Journal of Geophysical Research: Oceans, 112:C07017

Hickey BM (1998) Coastal oceanography of western North America from the tip of Baja California to Vancouver Island. In: Robinson AR, Brink KH (eds) The Sea, The Global Coastal Ocean: Regional Studies and Syntheses. Wiley, New York, pp 345–391

Iriarte JL, González HE (2004) Phytoplankton size structure during and after the 1997/98 El Niño in a coastal upwelling area of the northern Humboldt Current System. Mar Ecol Prog Ser 269:83–90

Ito S-I, Rose KA, Miller AJ, Drinkwater K, Brander KM, Overland JE, Sundby S, Curchitser E, Hurrell JW, Yamanaka Y (2010) Ocean ecosystem responses to future global change scenarios: a way forward. In: Global Change and Marine Ecosystems, Barange M, Field J, Harris R, Hofmann E, Perry I, Werner F (Eds.) Oxford University Press, pp. 287–322

Jacox MG, Alexander MA, Stock CA, Hervieux G (2019) On the skill of seasonal sea surface temperature forecasts in the California Current System and its connection to ENSO variability. Clim Dynam 53:7519–7533

Jacox MG, Fiechter J, Moore AM, Edwards CA (2015) ENSO and the California Current coastal upwelling response. J Geophys Res Oceans 120:1691–1702

Jacox MG, Hazen EL, Zaba KD, Rudnick DL, Edwards CA, Moore AM, Bograd SJ (2016) Impacts of the 2015–2016 El Niño on the California Current system: early assessment and comparison to past events. Geophys Res Lett 43:7072–7080

Jacox MG, Edwards CA, Hazen EL, Bograd SJ (2018) Coastal upwelling revisited: Ekman, Bakun, and improved upwelling indices for the U.S. West Coast. J Geophys Res Oceans 123:7332–7350

Jacox MG, Alexander MA, Siedlecki S, Chen K, Kwon Y-O, Brodie S, Ortiz I, Tommasi D, Widlansky MJ, Barrie D, Capotondi A, Cheng W, Di Lorenzo E, Edwards C, Fiechter J, Fratantoni P, Hazen EL, Hermann AJ, Kumar A, Miller AJ, Pirhalla D, Pozo Buil M, Ray S, Sheridan SC, Subramanian A, Thompson P, Thorne L, Annamalai H, Bograd SJ, Griffis RB, Kim H, Mariotti A, Merrifield M, Rykaczewski R (2020) Seasonal-to-interannual prediction of North American coastal marine ecosystems: forecast methods, mechanisms of predictability, and priority developments. Progress Oceanogr 183:102307

Kishi MJ, Kashiwai M, Ware DM, Megrey BA, Eslinger DL, Werner FE, Noguchi-Aita M, Azumaya T, Fuji M, Hashimoto S, Huang D, Izumi H, Ishida Y, Kang S, Kantakov GA, Kim H, Komatsu K, Navrotsky VV, Smith SL, Tadokoro K, Tsuda A, Yamamura O, Yamanaka Y, Yokouchi K, Yoshie N, Zhang J, Zuenko YI, Zvalisnky VI (2007) NEMURO—a lower trophic level model for the North Pacific marine ecosystem. Ecol Model 202:12–25

Lilly LE, Ohman MD (2018) CCE IV: El Niño-related zooplankton variability in the southern California Current System. Deep Sea Res Pt I 140:36–51

Lilly LE, Ohman MD (2021) Euphausiid spatial displacements and habitat shifts in the southern. Progress Oceanogr 193:102544

Mackas DL, Galbraith M (2002) Zooplankton community composition along the inner portion of Line P during the 1997–1998 El Niño event. Prog Oceanogr 54:423–437

Marchesiello P, McWilliams JC, Shchepetkin A (2003) Equilibrium structure and dynamics of the California Current system. J Phys Oceanogr 33:753–783

McGowan JA, Cayan DR, Dorman LM (1998) Climate-ocean variability and ecosystem response in the northeast Pacific. Science 281:210–217

McPhaden MJ, Busalacchi AJ, Cheney R, Donguy J-R, Gafe KS, Hapern D, Ji M, Julian P, Meyers G, Mitchum GT, Niiler PP, Picaut J, Reynolds RW, Smith N, Takeuchi K (1998) The tropical ocean-global atmosphere observing system: a decade of progress. J Geophys Res 103(14):169–14 (420)

Miller AJ, Song H, Subramanian AC (2015) The physical oceanographic environment during the CCE-LTER years: changes in climate and concepts. Deep-Sea Res 112:6–17

Nishikawa H, Curchitser EN, Fiechter J, Rose KA, Hedstrom K (2019) Using a climate-to-fishery model to simulate the influence of the 1976–1977 regime shift on anchovy and sardine in the California Current System. Prog Earth Planet Sci 6:9

Ohman MD, Barbeau K, Franks PJS, Goericke R, Landry MD, Miller AJ (2013) Ecological transitions in a coastal upwelling ecosystem. Oceanography 26:210–219

O'Reilly JL, Maritorena S, O'Brien MC, Siegel DA, Toole D, David Menzies D, Smit RC, Mueller JE, Mitchell BG, Kahru M, Chavez SP, Strutton P, Cota GF, Hooker SB, McClain CR, Carder KL, Müller-Karger F, Harding R, Magnuson A, Phinney D, Moore GF, Aiken J, Arrigo KR, Letelier R, Culver M (2000) SeaWiFS post-launch calibration and validation analyses, Part 3. NASA Tech. Memo. 2000–206892, 11, Hooker SB, Firestone ER (Eds.) NASA Goddard Space Flight Center

Overland JE, Alheit J, Bakun A, Hurrell JW, Mackus DL, Miller AJ (2010) Climate controls on marine ecosystems and fish populations. J Mar Syst 79:305–315

Politikos DV, Curchitser EN, Rose KA, Checkley DM, Fiechter J (2017) Climate variability and sardine recruitment in the California Current: a mechanistic analysis of an ecosystem model. Fish Oceanogr 27:602–622

Rayner NA, Parker DE, Horton EB, Folland CK, Alexander LV, Rowell DP (2003) Global analyses of sea surface temperature, sea ice, and night marine air temperature since the late nineteenth century. J Geophys Res 108:4407

Rose KA, Fiechter J, Curchitser EN, Hedstrom K, Bernal M, Creekmore S, Haynie A, Ito S, Lluch-Cota S, Megrey BA, Edwards CA, Checkley D, Koslow T, McClatchie S, Werner F, MacCall A, Agostini V (2015) Demonstration of a fully-coupled end-to-end model for small pelagic fish using sardine and anchovy in the California Current. Prog Oceanogr 138:348–380

Rykaczewski RR, Dunne JP (2010) Enhanced nutrient supply to the California Current Ecosystem with global warming and increased stratification in an earth system model. Geophys Res Lett 37:L21606

Schmidt DF, Amaya DJ, Grise KM, Miller AJ (2020) Impacts of shifting subtropical highs on the California and Canary Current Systems. Geophys Res Lett 47:e2020GL088996

Schwing FB, Palacios DM, Bograd SJ (2005) El Niño impacts on the California Current ecosystems. U.S CLIVAR Newsl 3:5–8

Seo H, Miller AJ, Norris JR (2016) Eddy-wind interaction in the California Current System: dynamics and impacts. J Phys Oceanogr 46:439–459

Shchepetkin AF, McWilliams JC (2005) The regional oceanic modeling system (ROMS): a split-explicit, free-surface, topography-following-coordinate ocean model. Ocean Model 9:347–404

Song H, Miller AJ, Cornuelle BD, Di Lorenzo E (2011) Changes in upwelling and its water sources in the California Current System driven by different wind forcing. Dyn Atmos Oceans 52:170–191

Song H, Miller AJ, McClatchie S, Weber ED, Nieto KM, Checkley DM (2012) Application of a data-assimilation model to variability of Pacific sardine spawning and survivor habitats with ENSO in the California Current System. J Geophys Res Oceans 117:C03009

Stock CA, John JG, Rykaczewski RR, Asch RG, Cheung WWL, Dunne JP, Friedland KD, Lam VWY, Sarmiento JL, Watson RA (2017) Reconciling fisheries catch and ocean productivity. Proc Natl Acad Sci 114:E1441–E1449

Thomas AC, Strub PT, Weatherbee RA, James C (2012) Satellite views of Pacific chlorophyll variability: comparisons to physical variability, local versus nonlocal influences and links to climate indices. Deep-Sea Res II 77–80:99–106

Tommasi D, Stock CA, Hobday AJ, Methot R, Kaplan IC, Eveson JP, Holsman K, Miller TJ, Gaichas S, Gehlen M, Pershing A, Vecchi GA, Msadek R, Delworth T, Eakin CM, Haltuch MA, Séférian R, Spillman CM, Hartog JR, Siedlecki S, Samhouri JF, Muhling B, Asch RG, Pinsky ML, Saba VS, Kapnick SB, Gaitan CF, Rykaczewski RR, Alexander MA, Xue Y, Pegion KV, Lynch P, Payne MR, Kristiansen T, Lehodey P, Werner FE (2017) Managing living marine resources in a dynamic environment: the role of seasonal to decadal climate forecasts. Prog Oceanogr 152:15–49

Turi G, Alexander M, Lovenduski N, Capotondi A, Scott J, Stock C, Dunne J, John J, Jacox M (2018) Response of oxygen and PH to ENSO of the California Current System in a high-resolution global climate model. Ocean Sci 14:69–86

Van Oostende N, Dussin R, Stock CA, Barton AD, Curchitser E, Dunne JP, Ward BB (2018) Simulating the ocean's chlorophyll dynamic range from coastal upwelling to oligotrophy. Prog Oceanogr 168:232–247

Venrick EL (2009) Floral patterns in the California Current: the coastal-offshore boundary zone. J Mar Res 67:89–111